Surface Science 257 (1991) 41–49
North-Holland

Incident ion energy effects on the secondary Rh^+ ion kinetic energy and azimuthal angle distributions from Rh{111}

G.P. Malafsky [1] and N. Winograd

Department of Chemistry, The Pennsylvania State University, University Park, PA 16802, USA

Received 5 April 1991; accepted for publication 9 May 1991

The nature of the collision cascade initiated by a bombarding ion beam strongly depends upon the kinetic energy of the ion beam. As the incident ion beam energy is lowered, the changes in the collision cascade cause a reduction in the total ejected particle yield, the ion fraction of the ejected particles, and the fraction of ejected clusters. We present the azimuthal angle and kinetic energy distributions of secondary Rh^+ ions from a clean Rh{111} sample bombarded with 250 and 3000 eV Ar^+ ion beams. These distributions show features associated with the lattice atomic arrangement and a previously unreported secondary ionization mechanism which arises from damage to the electronic structure of the lattice. The azimuthal angle and kinetic energy distributions exhibit substantial changes at low primary ion beam energy due to the diminution of the collision cascade.

1. Introduction

An ion beam impinging on a solid initiates a collision cascade which results in the ejection of substrate atoms into the vacuum [1,2]. The bombarding ion transfers a part of its momentum to the substrate atoms generating a series of collision sequences which extend several atomic layers deep into the solid and into a radius as many as ten atoms wide [1]. The physics of the particle–solid interaction forms the basis of the surface sensitive spectroscopies secondary ion mass spectrometry (SIMS) [3], energy and angle resolved neutral particle detection (EARN) [4], and sputtered neutral mass spectrometry (SNMS) [5].

The specific nature of the collision sequences depends upon the bombarding ion kinetic energy. Simulations of the collision cascade reveal that the complexity of the atom–atom collision sequences increases as the incident ion energy rises above a few hundred eV [1]. The changes in the collision cascade are reflected in the experimentally measured ejected particle distributions. Reducing the bombarding ion energy lowers the total ejection yield [6] and the fractional cluster yield [5]. In addition, the high-energy portion of the ejected particle kinetic energy distributions diminishes as the bombarding particle energy is reduced [7–9].

The SIMS, EARN, and SNMS distributions are often interpreted as an indication of the surface structure from a single-crystal sample. However, the ability to reconstruct the surface structure is sensitive to the primary ion energy. For example, the rising SIMS O^- intensity with increasing oxygen dosage on a W{100} target exhibited a slope change at the coverage where the oxygen formed an ordered overlayer [10]. This slope change was not observed for a 2000 eV incident ion energy but became steadily more distinct as the incident ion energy was lowered to 150 eV. Also, the relative yields of cluster ions, such as $NiCO^+$ and Ni_2CO^+ from CO/Ni{001}, has been considered to be representative of the adsorbate bonding site [11]. At a bombardment energy of several keV, the cluster ion can be formed above the surface from non-contiguous

[1] Present address: Naval Research Laboratory, Code 6114, Chemistry Division, 4555 Overlook Ave., Washington, DC 20375-5000, USA.

atoms preventing their correlation to the surface structure. At a low incident ion energy, they are more likely to form from nearest-neighbor pairs [12] and may be better correlated to the actual bonding arrangement. In addition, the measured surface symmetry of a single-crystal sample depends upon the primary ion energy. The close-packed surface of a fcc metal, such as Au{111}, has six equivalent open azimuthal directions. However, with a primary ion energy of 10 keV the ejected azimuthal distributions show a disparity in the two azimuthal intensities while this disparity is greatly reduced when the primary ion energy is 400 eV [13]. The difference in azimuthal intensities arises from the involvement of the second and third layer atoms in the collision cascade.

Moreover, the secondary ionization process depends upon the bombarding ion energy. The fraction of the ejected particles which are ionized increases by an order of magnitude for some metals as the bombarding ion energy increases from 100–10 000 eV [14]. The sensitivity of the secondary ion yield to the energy deposited in the crystal is even more apparent for multiply charged ions [2]. These ions are known to result from violent collisions.

In a separate paper [15], we described the difference between the kinetic energy and azimuthal angle distributions of the secondary Rh^+ ions and Rh neutral particles ejected from a clean Rh{111} sample by Ar^+ ion bombardment. The Rh^+ ion distributions show additional structure which is not present in the Rh neutral particle distributions. We proposed that the additional structure arises from certain collision sequences initiated by the bombarding ion beam which sufficiently disrupt the electronic structure of the lattice such that electronic excitations created in the collision cascade survive until the particle has ejected from the substrate. These electronic excitations are usually ignored in models of the secondary ionization process from metals (e.g., the tunneling model) because of the very short lifetimes of the excitations in an unperturbed metal lattice [2].

In this study, we examine the influence of the primary ion energy on the ejected Rh^+ ion distributions from the clean Rh{111} crystal. The secondary ion kinetic energy and azimuthal angle distributions are compared for bombarding ion energies of 250 and 3000 eV. The changes in these distributions are correlated with the variance in the collision cascade. Also, we assess the effect of the low bombarding ion energy on the preponderance of collisional events in contributing to the ionization process.

2. Experimental

The experimental apparatus has been described in detail elsewhere [16] and will be only briefly mentioned in this section. The ultrahigh vacuum (UHV) chamber has a base pressure of $< 1 \times 10^{-10}$ Torr. It is equipped with a primary ion beam source, a crystal manipulator, a secondary ion detector apparatus, and a LEED/Auger spectroscopy unit.

The primary ion beam system is capable of producing a mass-filtered Ar^+ beam of 0.72 μA at 500 eV into a 1 mm diameter spot [17]. This is accomplished by passing the beam through a set of transport optics designed specifically for the high-current and low-energy ion beam. Since the gun efficiently transports low energy beams, we are able to use focussed ion beams with energies lower than are available to most researchers. The pressure in the main chamber is approximately 8×10^{-9} Torr while operating the primary ion beam system. However, the pressure rise of gases other than argon is less than 8×10^{-10} Torr. A low background of residual gases is important since the reactive clean Rh metal quickly adsorbs contaminants.

The detected polar angle is measured from the axis perpendicular to the sample plane. It is varied by rotating the secondary ion detector apparatus about the sample. The polar angle resolution is defined by a 2 mm aperture at the entrance of the detector apparatus and is approximately 10°. The azimuthal angle is measured in the crystal plane and is varied by rotating the crystal on the manipulator about the axis perpendicular to the sample surface. The azimuthal resolution is a function of the polar angle [11] and is

about 14° at a polar angle of 45° and is about 11° at a polar angle of 65°.

The secondary ion kinetic energy spectra are acquired by supplying a 0 to 50 V bias to the collector optics and the 90° spherical electrostatic energy analyzer. The linear voltage ramp maintains a constant band pass of the energy analyzer and a constant focal plane for the collector ion optics. The bias voltage determines the absolute pass energy of the secondary ion detector apparatus. The zero reference point of the energy analyzer is calibrated with thermally desorbed K^+ ions from the sample during a high temperature anneal. The energy resolution of the collection system is about ±2 eV.

An IBM-AT computer controls the selection of the detected mass, energy, and angle. Due to the very low signal level (< 10 cps), the signal at each data point is counted for about 30 s in order to obtain an acceptable signal to noise level. The pulses from the channeltron electron multiplier (CEM) are filtered by a 100 MHz amplifier–discriminator and then converted into slower TTL pulses which are counted with a 5 MHz pulse counter.

The Rh{111} crystal was oriented to ±0.5° and polished to a mirror finish by Johnson-Matthey. It was cleaned by cycles of sputtering with a 1 keV Ar^+ beam of 1 μA current which is rastered over the surface for 5 min, followed by a 10 min anneal at 700°C with a 30 s O_2 dose to remove carbon and a 30 s flash to 950°C to desorb the oxygen. Carbon is a troublesome contaminant since it continues to diffuse to the surface from the bulk until it is depleted [18]. Hundreds of sputter/anneal cycles were required to clean the new crystal. The presence of carbon is monitored by the SIMS Rh_2C^+/Rh_2^+ ratio. On the clean surface, only a slight RhC^+ peak and the high ion yield species Na^+, Al^+, and K^+ are present in the SIMS spectrum as seen in fig. 1. After annealing, a sharp (1 × 1) LEED pattern indicated the surface was well ordered.

The primary ion fluence is low in order to maintain the surface order during an experiment. For the 3000 eV ion beam, we use a current of 100–200 pA in a 1–1.5 mm diameter spot. A higher current of 200–400 pA is used for the 250

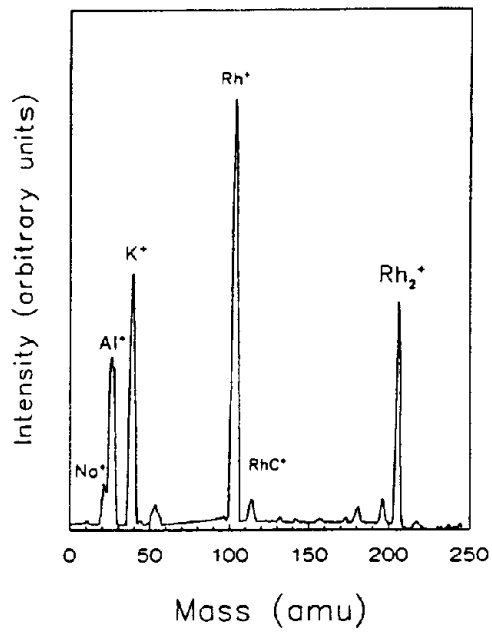

Fig. 1. SIMS spectrum of the clean Rh(111) sample. The spectrum is normalized to the Rh^+ peak.

eV beam because of the lower ion yield and the lower surface damage at this energy. In both cases, the primary Ar^+ beam bombards the sample at normal incidence. A typical signal level for the 3000 eV beam is 10 cps whereas for the 250 eV beam the signal level is 4 cps. The total time of an experiment was limited to 30 min to prevent serious surface damage and to prevent the adsorption of contaminants which could alter the ejected ion distributions. We observed small quantities of contaminants by SIMS ($RhOH^+$, $RhCO^+$) after about 1 h of exposure to the ion beam. An experiment was started when the crystal had cooled to less than 200°C. The ejection yield does not change appreciably below 400°C [3] and the azimuthal spectra are the same at 200 and 50°C.

3. Results and discussion

The Rh{111} surface has a sixfold symmetry which is reduced to a threefold symmetry by the interaction of the second layer of atoms. The three major azimuthal directions are labeled in

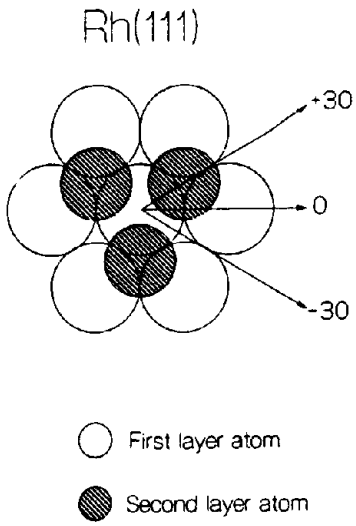

Fig. 2. The atomic arrangement of the first and second layers of the Rh(111) surface. The three principal azimuthal directions are labeled as $\Phi = -30°, 0°, +30°$.

fig. 2 as $\Phi = -30°$, 0°, and $+30°$. The $\pm 30°$ azimuths are the two relatively open directions along which ejecting atoms are preferentially channeled [19]. In this section, we present the azimuthal angle and kinetic energy distributions of the ejected Rh^+ ions for the primary Ar^+ ion energies of 250 and 3000 eV.

3.1. Azimuthal angle distributions

The azimuthal angular distributions for incident Ar^+ ion beam energies of 250 and 3000 eV are shown in fig. 3 at a polar angle of detection of 45° for three different secondary ion energies. For the 8 eV secondary Rh^+ ions, the $-30°$ azimuthal peak has a higher intensity than the $+30°$ azimuthal peak for both bombardment energies. This is also true for the ejected neutral atom distributions [19] and demonstrates the influence of the second layer atoms in the collision cascade. Molecular dynamics simulations of the ejection process show that a second layer atom can move towards the surface causing a first layer atom to eject along the $-30°$ azimuth. As the secondary particle energy increases to 15 eV, the disparity in the azimuthal intensities decreases.

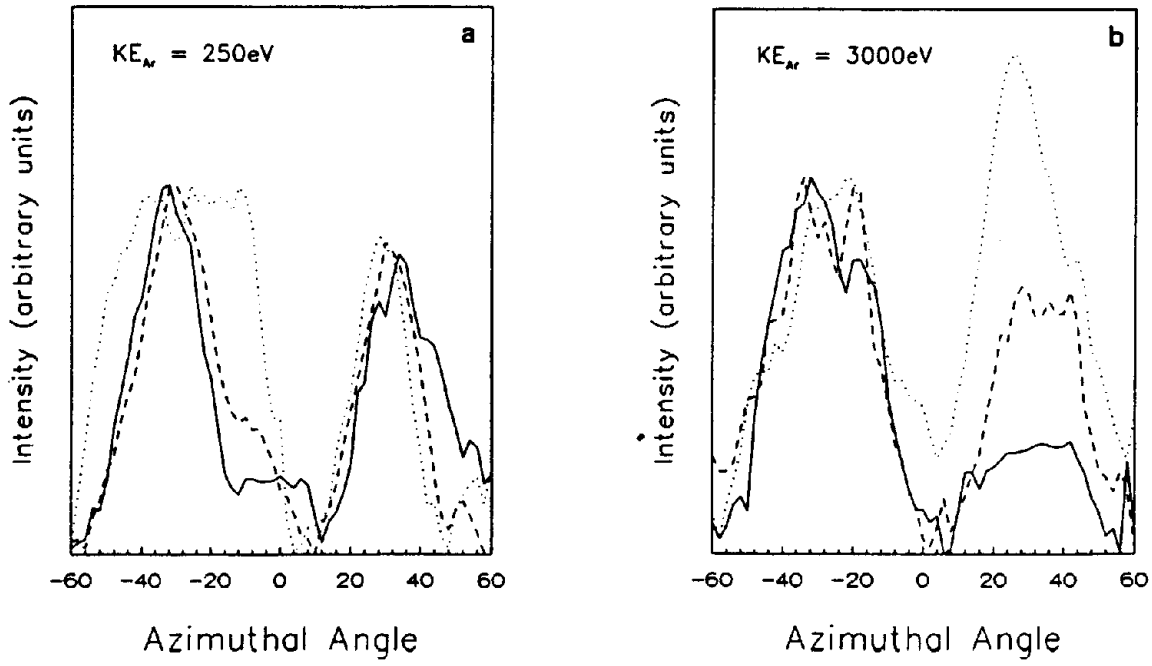

Fig. 3. Secondary Rh^+ ion azimuthal angle distributions at a polar angle of detection of 45° for Rh^+ ion kinetic energies of 8 eV(———), 15 eV (— — —), and 25 eV(· · · · · ·). The spectra are normalized to the peaks at $\Phi = -30°$. The incident Ar^+ ion kinetic energy is (a) 250 eV, and (b) 3000 eV.

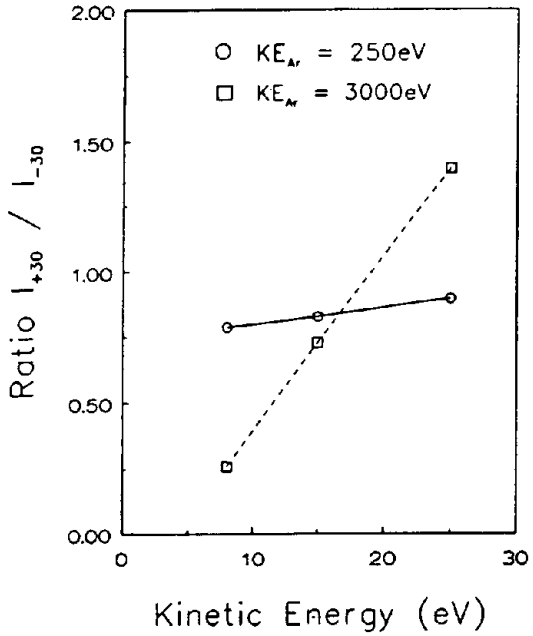

Fig. 4. The azimuthal angle intensity ratio, I_{+30}/I_{-30}, versus the secondary Rh^+ ion kinetic energy at a polar angle of 45° for incident Ar^+ ion kinetic energies of 250 and 3000 eV.

Presumably, the higher-energy secondary particles are ejected early in the collision cascade before the collision sequence involving the second layer atom is generated [19]. However, for an incident ion energy of 3000 eV, the intensity of the +30° azimuth is larger than the intensity of the −30° azimuth at a Rh^+ energy of 25 eV. This is not true for the Rh neutral particle distributions nor for an incident Ar^+ ion energy of 250 eV.

The value of the azimuthal intensity ratio, I_{+30}/I_{-30} is displayed in fig. 4 versus the secondary ion energy for the two bombardment energies. I_{+30}/I_{-30} changes very little for the 250 eV incident ion energy but is strongly dependent on the Rh^+ energy for the 3000 eV incident ion energy. In particular, the value of I_{+30}/I_{-30} is much closer to unity at an incident ion energy of 250 eV for the 8 eV Rh^+ ions which suggests that there are fewer collision sequences at the lower bombardment energy which involve a second-layer atom ejecting a first layer atom along the −30° azimuth. In addition, I_{+30}/I_{-30} does not exceed unity for the 25 eV Rh^+ ions for the 250 eV incident ion energy. Previously, we proposed that the increase in I_{+30}/I_{-30} to a value greater than unity at an incident ion energy of 3000 eV revealed the influence of collisional processes in the secondary ionization mechanism [15]. Therefore, the diminished expanse of the collision cascade at an incident ion energy of 250 eV is shown by both the weak dependence of I_{+30}/I_{-30} on the secondary Rh^+ ion energy and by a value of I_{+30}/I_{-30} less than unity for 25 eV Rh^+ ions.

3.2. Kinetic energy distributions

The kinetic energy spectra of the Rh^+ ions desorbed by 250 eV and 3000 eV Ar^+ ion beams are shown in figs. 5–7. The double-peaked structure of these spectra is unusual since the energy distributions of Rh neutral particles from Rh{111} [19], Ni^+ ions from Ni{100} [11], and Cu^+ ions from Cu{100} [20] show only a single peak. The neutral particle distributions typically peak near an energy of $E_b/2$, where E_b is the surface binding energy, and fall off as KE^{-2} [3]. The corresponding ion distributions are often similar in shape but peak at a higher energy due to image force effects and velocity dependent neutralization mechanisms [3]. In contrast to the normal incidence ion beam used in this study, a double-peaked structure has been reported when the surface is bombarded at a glancing angle where recoil scattering is possible [21].

We believe that the origin of the second peak (Rh^+ energy of 22–28 eV) arises from collision sequences which disrupt the electronic structure of the lattice thereby allowing excitations to survive until the particle has ejected from the substrate [15]. These collision sequences are rare but have a high yield of ejected particles [1]. Since the overall ion yield from clean metal surfaces is quite low, it is possible that the high ejected particle yield and the higher ionization probability from these rare collision sequences can contribute a significant fraction of the measured ion signal. If this sort of collisional mechanism is occurring, it is likely that the kinetic energy spectra will be dependent upon the kinetic energy of the bombarding particle and the polar angle of ejection of the secondary Rh^+ ions.

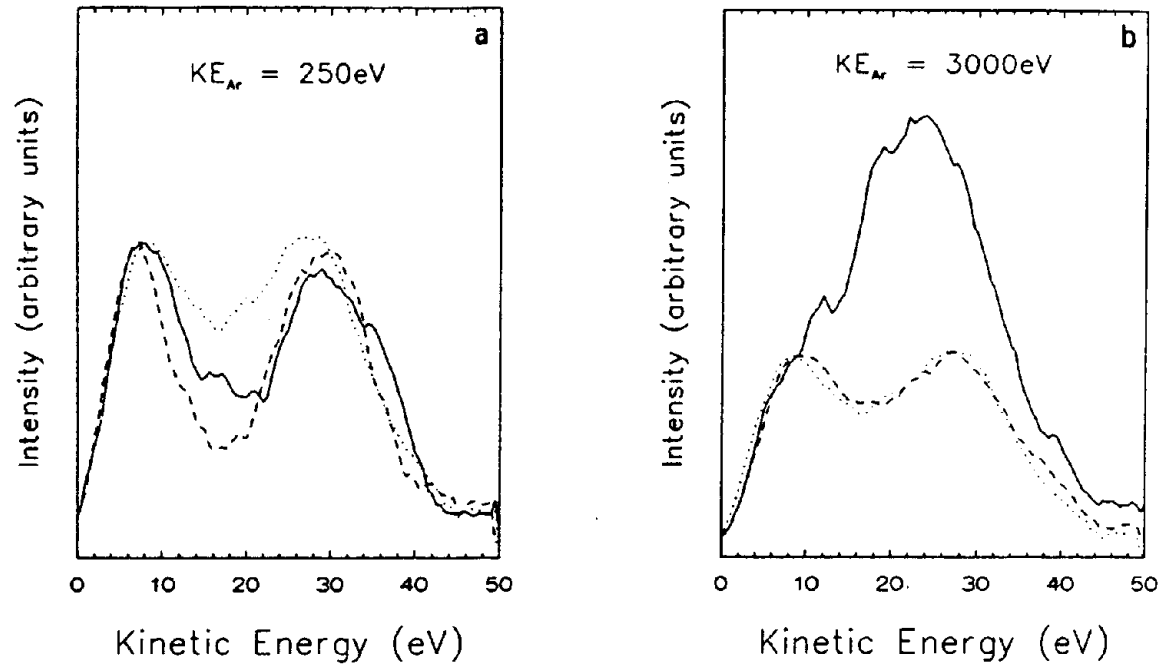

Fig. 5. Kinetic energy distributions of the secondary Rh^+ ions for the three principal azimuthal directions of $\Phi = -30°$ (——), 0° (— — —), +30° (·····). The curves are normalized to the peak at 8 eV. The polar angle of detection is 45°. The incide Ar^+ ion kinetic energy is (a) 250 eV, and (b) 3000 eV.

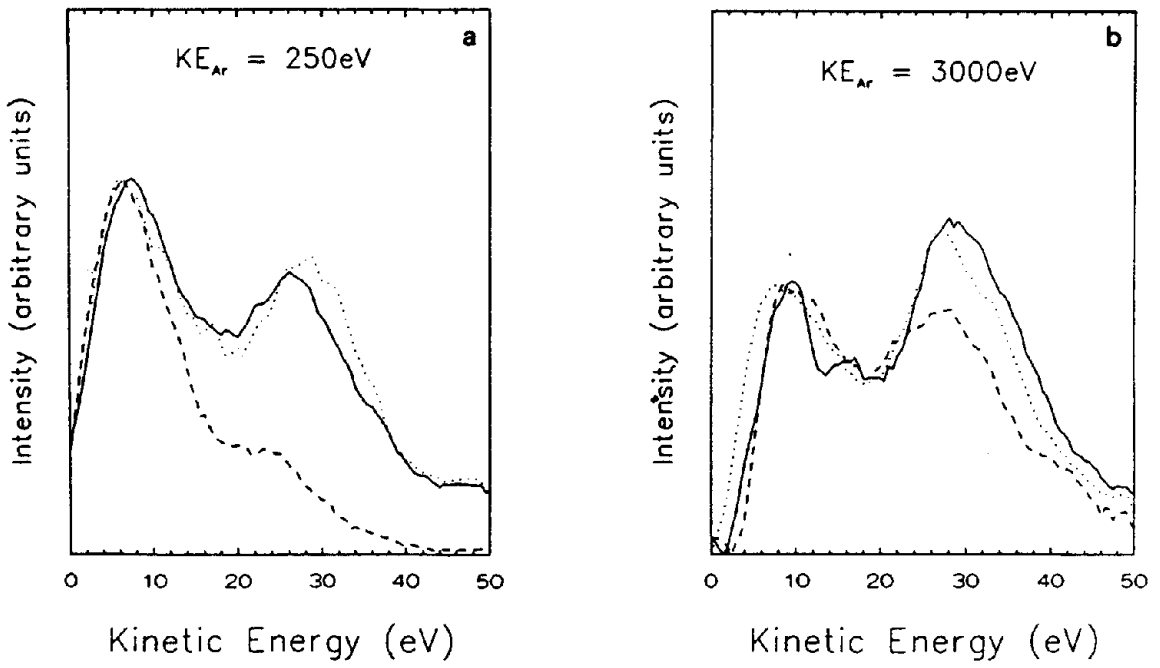

Fig. 6. Same as in fig. 5 except that the polar angle is 55°.

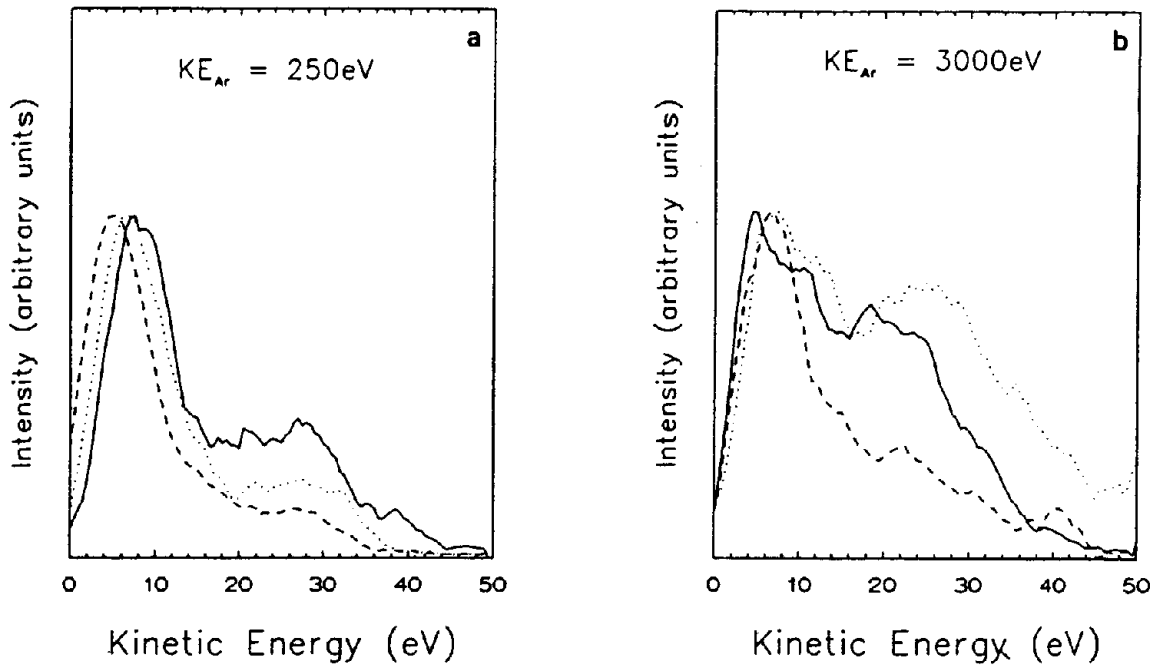

Fig. 7. Same as in fig. 5 except that the polar angle is 65°.

The high-energy peak has its maximum value relative to the low-energy peak at a polar angle of 45°. Also, for the 3000 eV incident particle, the high-energy peak predominates in the +30° azimuth as a result of the interaction of the second-layer atoms. The relative intensity of the

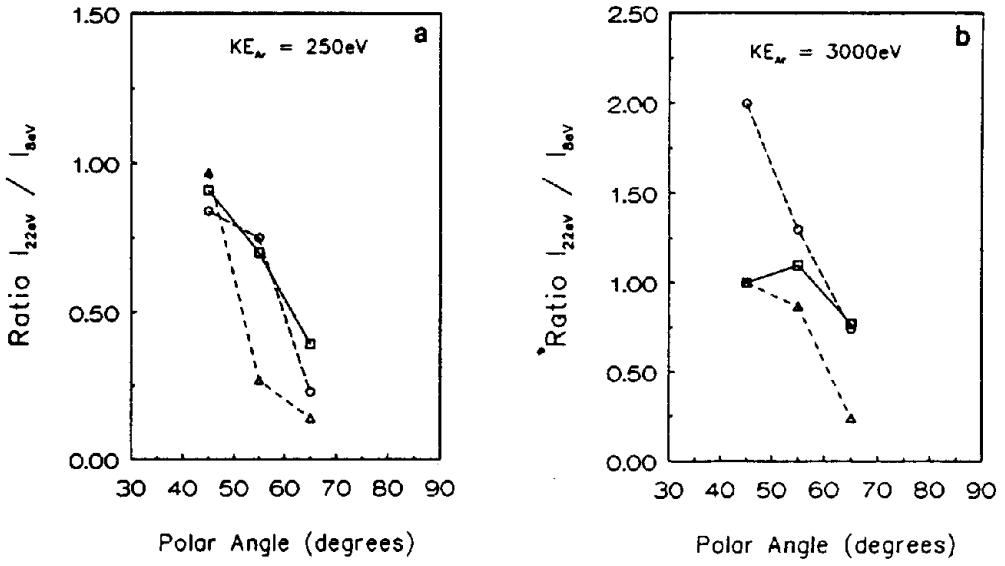

Fig. 8. The ratio of the intensities of the high-energy to the low-energy peaks in the kinetic energy spectra of the secondary Rh^+ ions, $I_{22\,eV}/I_{8\,eV}$, for the three principal azimuthal angle directions of $\Phi = -30°$ (———), 0° (— — —), +30°(· · · · · ·). The incident Ar^+ ion kinetic energy is (a) 250 eV, and (b) 3000 eV.

high energy peak diminishes as the polar angle increases due to an increase in blocking of the ejecting particles by surface atoms. The decay in the intensity of the high-energy peak with polar angle is most rapid for the 0° azimuth because of the presence of a nearest-neighbor atom along this azimuthal direction.

The ratio of the intensity of the high energy peak to the intensity of the low energy peak, I_h/I_l, is shown in fig. 8 for the two incident ion energies. The value of I_h/I_l is always lower for the 250 eV bombardment energy. Also, the relative intensity of the high-energy peak is nearly the same for the ±30° azimuths at a bombarding ion energy of 250 eV. These data reflect the diminution of the collision cascade at the low primary ion energy. The decrease in the energy deposited in the crystal by the low-energy incident ion results in an abatement of the collision sequences which have a high ejection yield and severely damage the lattice. These are the collision sequences which are likely to stimulate the collisional ionization mechanism. Therefore, the secondary ions created by the collisional ionization mechanism contribute less to the total ion yield. In fact, simulations of low-energy bombardment show the reduced expanse of the collision cascade. Both the penetration depth of the primary ion [22] and the ejection yield of second-layer atoms [1] are strongly attenuated at low primary ion energies.

4. Conclusions and summary

The azimuthal angle and kinetic energy distributions of Rh^+ ions ejected from a clean Rh{111} sample are strongly affected by the kinetic energy of the incident Ar^+ ion beam. The expanse of the collision cascade is reduced at a bombarding ion beam energy of 250 eV compared to 3000 eV. This is evident by the reduction in the intensity disparity along the +30° and −30° azimuths for low kinetic energy Rh^+ ions since this disparity arises from the involvement of second-layer atoms in the ejection process during the collision cascade. In addition, we have shown that the distributions exhibit features which are not present in the Rh neutral particle distributions and may arise from the influence of certain collision sequences which significantly disrupt the electronic structure of the lattice and thereby contribute to the secondary ionization process. The azimuthal angle distributions exhibit a change in the relative intensities along the +30° and −30° azimuths from $I_{-30} > I_{+30}$ for low-energy Rh^+ ions to $I_{-30} < I_{+30}$ for high-energy Rh^+ ions. The Rh^+ ion kinetic energy distributions show a double peaked structure which has not been previously observed. The diminution of the collision cascade with the 250 eV Ar^+ ion beam reduces the preponderance of these special features.

Finally, these data suggest additional experimental and theoretical studies to understand the microscopic mechanisms of secondary ionization. For example, it should be possible to use molecular dynamics simulations of the collision cascade to identify the types of collision sequences which lead to enhanced ionization [1]. Also, the structures in the distributions from the enhanced ionization collision sequences are not observed in the secondary ion distributions from Ar^+ ion beam bombarded Ni{100} [11] or Cu{100} [20] suggesting that this ionization mechanism may depend upon the electronic structure of the target or the masses of the bombarding ions and the target.

Acknowledgements

We gratefully acknowledge the financial assistance provided by the National Science Foundation and the Office of Naval Research. Also, we wish to thank R. Blumenthal, K. Caffey, and R. Braun for their assistance with this work.

References

[1] D.E. Harrison, Jr., CRC Rev. Solid State Mater Sci. 14 (1988) S1.
[2] G. Blaise and A. Nourtier, Surf. Sci. 90 (1979) 495.
[3] N. Winograd, Prog. Solid St. Chem. 13 (1982) 285.
[4] P.H. Kobrin, G.A. Schick, J.P. Baxter and N. Winograd. Rev. Sci. Instrum. 57 (1986) 1354.
[5] W. Gerhard and H. Oechsner, Z. Phys. B 22 (1975) 41.

[6] H.E. Roosendaal, in: Sputtering by Particle Bombardment I, Ed. R. Behrisch (Springer, New York, 1981) p. 244.
[7] R.G. Hart and C.B. Cooper, Surf. Sci. 94 (1980) 105.
[8] C.B. Cooper and H.A. Hamed, Surf. Sci. 143 (1984) 215.
[9] R.A. Brizzolara, C.B. Cooper and T.K. Olson, Nucl. Instrum. Methods B 35 (1988) 36.
[10] M.L. Yu, J. Vac. Sci. Technol. 15 (1978) 668.
[11] R.A. Gibbs, S.P. Holland, K.E. Foley, B.J. Garrison and N. Winograd, J. Chem. Phys. 76 (1982) 684.
[12] K.E. Foley and N. Winograd, Surf. Sci. 122 (1982) 541.
[13] W. Symczak and K. Wittmaack, Nucl. Instrum. Methods 194 (1982) 561.
[14] K. Wittmaack, Surf. Sci. 53 (1975) 626.
[15] G.P. Malafsky and N. Winograd, in: SIMS VII, Ed. A. Benninghoven (Wiley, New York, 1990) p. 37.
[16] R.A. Gibbs and N. Winograd, Rev. Sci. Instrum. 52 (1981) 1148.
[17] G.P. Malafsky and N. Winograd, Rev. Sci. Instrum. 59 (1988) 1294.
[18] L.A. DeLouise and N. Winograd, Surf. Sci. 138 (1984) 417.
[19] J. Singh, C.T. Reimann, J.P. Baxter, G.A. Schick, P.H. Kobrin, B.J. Garrison and N. Winograd, J. Vac. Sci. Techol. A 5 (1987) 1191.
[20] R. Braun and N. Winograd, unpublished results.
[21] M.W. Thompson, Philos. Mag. 18 (1968) 377.
[22] M.H. Shapiro and T.A. Tombrello, Nucl. Instrum. Methods B 18 (1987) 355.